Received: 2 January 2024 | Revised: 26 March 2024 | Accepted: 11 April 2024

DOI: 10.1002/vjch.202400003

RESEARCH ARTICLE

# Properties and corrosion protection of polypyrrole prepared by electrochemical polymerization on aluminum

**Le Van Khoe**[1] | **Ha Manh Hung**[2] | **Le Minh Duc**[3] | **Ngo Xuan Luong**[1] | **Nguyen Thi Bich Viet**[4] | **Vu Thi Huong**[4] | **Doan Thi Yen Oanh**[5] | **Vu Quoc Trung**[4]

[1]Faculty of Natural Sciences, Hong Duc University, Thanh Hoa City, Vietnam

[2]Faculty of General Education, Hanoi University of Mining and Geology, Hanoi, Vietnam

[3]Department of Environmental Engineering, Branch of National Institute of Occupational Safety and Health and Environmental Protection in Central of Vietnam, Da Nang, Vietnam

[4]Faculty of Chemistry, Hanoi National University of Education, Cau Giay, Hanoi, Vietnam

[5]Publishing House for Science and Technology, Vietnam Academy of Science and Technology, Cau Giay, Hanoi, Vietnam

**Correspondence**
Vu Quoc Trung, Faculty of Chemistry, Hanoi National University of Education, 136 Xuan Thuy, Cau Giay, Hanoi 10000, Vietnam.
Email: trungvq@hnue.edu.vn

**Funding information**
Vietnam National Foundation for Science and Technology Development (NAFOSTED), Grant/Award Number: 104.02-2019.327

**Abstract**

In a one-step procedure that did not require any surface preparation, polypyrrole (PPy) films doped with 3-nitrosalicylic acid (3Nisa) became effectively electropolymerized on the aluminum substrate in aqueous solutions. Fourier transform infrared, scanning electron microscopy, and thermal gravimetric analysis were used to analyze the properties of PPy-based films. Open circuit potential (OCP), electrochemical impedance spectroscopy, Tafel polarization, and salt spray tests were used to study the corrosion-resistant efficiency of the coatings. The as-prepared PPy films performed corrosion resistance on aluminum in the 3% NaCl solution. However, the PPy films prepared in the 0.01 M solution of 3Nisa showed the best protection ability on aluminum. The self-healing characteristic of the PPy films was recorded by varying the potential in the OCP measurement. The findings indicate the potential of using 3-nitrosalicylic acid-doped PPy films for applications as anti-corrosion coatings for aluminum.

**KEYWORDS**

3-nitrosalicylic acid, aluminum, corrosion protection, polypyrrole, self-healing

## 1 | INTRODUCTION

Corrosion protection for metal/alloy structures, especially those immersed in seawater is extremely challenging and expensive work. To protect metals/alloys from corrosion, three main strategies can be applied, namely, cathodic protection, anodic protection, and protective coatings. The application of corrosion inhibitor-doped conducting polymers (CPs) on metals/alloys often provides multi-protection, both passive and active protection for metal/alloy surfaces to be protected.[1–5] These CPs such as polyaniline (PANI), polypyrrole (PPy), polythiophene (PT), etc. are widely studied and used for their excellent electronic behaviors and environmental stability.[6–8] Although polyaniline is the most studied conducting polymer due to its different oxidation states, polypyrrole is a good alternative because it is less hazardous than polyaniline and still has similar properties.

Lately, self-healing coating systems have emerged as smart and promising coatings for corrosion protection.[9,10] The self-healing property of a system is its ability to repair its own defects, often occurring after mechanical damages[11] or other defects,[12] by releasing active agents into the defect area.[13] The self-healing effect is often triggered by a change in pH, ionic strength,[14] or a change in potential.[12]

One of the approaches to achieve active protection is to use coatings embedded by nano/microcapsules loaded with various corrosion inhibitors that are intelligently released and then provide a self-healing effect.[12]

Active agents such as phosphate, molybdate, salicylate, oxalate, 3-nitrosalicylate, etc. have been usually chosen as self-healing agents because they can be used as counter-

anions for the polymeric backbone of the CPs. Among the mentioned self-healing agents, a greatly effective corrosion inhibitor for zinc was 3-nitrosalicylic acid (3Nisa).[15] Paliwoda-Porebska et al. studied the release mechanism of 3Nisa as a corrosion inhibitor doped in polypyrrole coatings electrodeposited on a zinc substrate in an aqueous solution. The OCP results proved that doping 3Nisa can considerably enhance the corrosion inhibition efficacy of PPy films for zinc substrate, which could be credited to chelate complex formation with Zn(II). However, the mobility of 3Nisa anions was not sufficient to protect zinc for an extended period. The authors also used SKP measurements to evaluate the cathodic delamination of this 3Nisa-doped PPy coating on zinc. The result showed that for a non-immersed sample with a larger defect, no corrosion inhibition was observed in the defect and in the delaminated area.

The active agent 3Nisa was also encapsulated in the PANI shell via a mini-emulsification method and its redox-responsive self-healing against corrosion was investigated by Rohwerder et al.[16] The results showed that this core-shell system displayed a remarkably switchable permeability to release the active agent into the electrolyte or store it inside the capsule. The potential change concurrent with delamination along the interface constituted the trigger signal. The PANI shell's permeability was activated by a reduction in the potential of the delaminated area, stopping both the active corrosion and the delamination.

Most recently, Yin et al.[17] used it as counter-anions in the electrodeposited PPy coating with entrapped neutral inhibitor molecules such as $\beta$-cyclodextrine, benzotriazole, and 8-hydroxyquinoline on electrochemically pretreated Zn surfaces. The results revealed that such coatings had the ability to passivate large corroding defects via a smart release in which 3Nisa was only leached in small amounts while entrapped neutral inhibitors were released in sufficient amounts to passivate the defects and the delaminated interfaces. These potential-trigged releases led to an increase in the corrosion potential in the defect by more than 200 mV. The inhibition mechanism was proposed as a synergy between the anodic polarization by re-oxidizing PPy and the effect of inhibitors.

Kanwal et al. have studied the corrosion protection behavior of epoxy blended sulfonate-doped polyaniline and polypyrrole coatings deposited on aluminum alloy AA2219-T6 substrates. Sulfonate doped-PANi and -PPy were synthesized by oxidative polymerization. An appropriate quantity of organic fillers: p-toluene sulfonic acid (p-TSA), camphor sulfonic acid (CSA) and sulfosalicylic acid (SSA), were mixed with the corresponding conductive polymers (CPs). Acid-doped polyaniline (PANi) and polypyrrole (PPy) were blended in epoxy matrices and coatings were applied on AA2219-T6 to assess the passivation of the metal surface towards corrosion. In this study, polypyrrole and polyaniline were used as particle fillers in epoxy matrix enhance the corrosion protection on Al substrate sucessfully.[18]

In Vietnam, aluminum alloys are popular in daily using. It is so important to enhance the corrosion protection ability of aluminum substrate. However, there are only a few reports on the direct preparation of PPy on aluminum or aluminum alloys using 3Nisa as dopants for corrosion protection. Choosing 3Nisa could be another alternative to widen the application of PPy film on Al alloy for corrosion protection.

In this article, we focused on the electropolymerized synthesis of PPy on Al substrates using 3Nisa as a dopant at various concentrations and investigated the ability of these coatings to protect Al substrates against corrosion.

## 2 | EXPERIMENTAL METHODS

### 2.1 | Chemicals and materials

Aluminum (aluminum alloy A5052, Al > 97%, purchased in Vietnam market). Each aluminum bar measured 150 mm × 50 mm × 1 mm. SiC sheets were used in various roughnesses, including 600, 800, 1000, 1200, and 1500, to mechanically polish and enhance the smoothness of the aluminum bars' surface. The aluminum substrate was subsequently degreased in an ultrasonic bath during 5 min with acetone, rinsed with distilled water, and then finally dried at room temperature under nitrogen flow.

Pyrrole monomer (Py) (+98%) and 3-nitrosalicylic acid (+98%) were purchased from Sigma-Aldrich. Before each usage, oxidized compounds, or oligomer components, which are by-products of the self-polymerization of pyrrole monomers, were eliminated through the distillation process. This step is essential to separate the mentioned side products and avoid them becoming mechanically attracted to the PPy film during the formation on the aluminum electrode and damaging the PPy film. The rod was then placed in no-light condition at 0 °C with the electrolyte solution with deionized water and pre-prepared components.

### 2.2 | Preparation of polypyrrole films on aluminum electrode

PPy films on Al samples (75 $cm^2$) were obtained by applying constant current of 0.9 mA in 30 min. The Zahner workstation potentiostat/galvanostat model (Zennium, Germany) was used to control the current/potential of polymerization. Three-electrode cell was used. The working, counter, and reference electrodes were aluminum, Pt gauze, and the Ag/AgCl electrode (SSE), respectively.

Monomer pyrrole solution was prepared with different concentrations of 3-nitrosalicylic acid as dopant anions (Table 1).

**TABLE 1** Component of the solutions used in electropolymerization.

| Solution/sample | 3-Nitrosalicylic acid | Pyrrole |
|---|---|---|
| A1 | 0.005 M | 0.1 M |
| A2 | 0.010 M | 0.1 M |
| A3 | 0.020 M | 0.1 M |

## 2.3 | Characterization of the PPy films

In atmosphere conditions, Ghimashu-50H performed thermal gravimetric analysis (TGA) at a scan rate of 10 °C $min^{-1}$. Raman and FT-IR spectroscopies were employed to determine the chemical structure of PPy films. A laser Raman spectrophotometer (Ramalog 9I, USA) was employed to record Raman spectra. The Prestige −21 (Shimadzu) was employed for FT-IR spectroscopy. Finally, the SEM images were captured using the SEMHITACHI-4800 at 10 keV energy.

## 2.4 | Corrosion protection test

The assessment of their anticorrosive properties was involved the measurement of open circuit potentials (OCP) and polarization curves (Tafel plot) in 3% NaCl solution, as well as electrochemical impedance spectroscopy (EIS) in 3% NaCl with Zennium (Zaehner, Germany). 3 electrode-cell was used in all electrochemical tests. Pt gauze was counter electrode and the Ag/AgCl electrode (SSE) was used as reference electrode.

EIS measurements were performed on the PPy films at different DC potentials (referred to as $E_{dc}$) using 5 mV AC at frequencies ranging from 100 kHz to 0.1 Hz.

# 3 | RESULTS AND DISCUSSION

## 3.1 | Electropolymerization of doped PPy on aluminum

Figure 1 depicts the potential versus time curves of doped PPy films on aluminum produced at a 0.9 mA $cm^2$ current density in a solution diluting 0.1 M pyrrole monomer with varying concentrations of 3-nitrosalicylic acid (Table 1).

The properties of resulting PPy sheets include thin, smooth, black, and homogenous. As seen in Figure 1, As the concentration of 3-nitrosalicylic acid increased, the synthesis potential of polypyrrole on the aluminum substrate increased.

The more stable passivation layer was formed leading to an increase in the resistance of the passive film. It led to the increasing of oxidation potential of PPy.

As a result, the synthesis potential increases when the applied current is constant. In each PPy sample, over time, the thickness of the formed PPy film also increases, leading to an increase in film resistance and an increase in the synthesized potential with time.

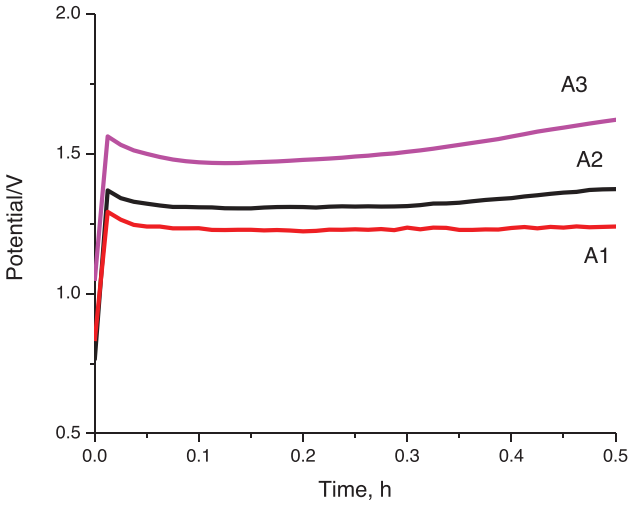


**FIGURE 1** The polarization curves versus time of electropolymerization of PPy on aluminum in different concentration solutions of 3-nitrosalicylic acid and 0.1 M pyrrole.

## 3.2 | SEM images of doped PPy films

Figure 2 illustrates the doped PPy films' morphology in both cases, with and without CSA dopants and molybdate anion. Doped PPy films were shown to have a characteristic structure with homogeneously dispersed cauliflower-shaped particles, as reported in references 15, 19, 20. The film's thick structure proved superior at protecting the metal from corrosion. No influence on the morphology of PPy films was recorded by the concurrent presence of salicylate anions.

## 3.3 | Raman spectra

Scattering Raman spectra of A1, A2, and A3 are shown in Figure 3. Besides the notion of the oxidizing state of PPy, there is also a modest change in the Raman shift in the doped PPy films' spectra produced in various conditions (Figure 3 and Table 2). Regarding the presence of physical contact in doped PPy films, this conclusion could correspond with the prior reported polarization potential of PPy films.

The high intensity peaks from 1572 to 1590 $cm^{-1}$, for example, represented conjugative backbone C—C=C stretching, whereas the 1368–1381 $cm^{-1}$ peak represented N—C ring stretching. Recording respectively at 1047–1080 $cm^{-1}$ and 1224–1236 $cm^{-1}$ were associated with N—H in-plane bending peak and C—C stretching peak.[21,22] Ring deformation and C—H out-of-plane deformation were correlated to the peaks at 931–939 $cm^{-1}$.[21] Table 2 compares the specific value in the Raman spectra of doped PPy films

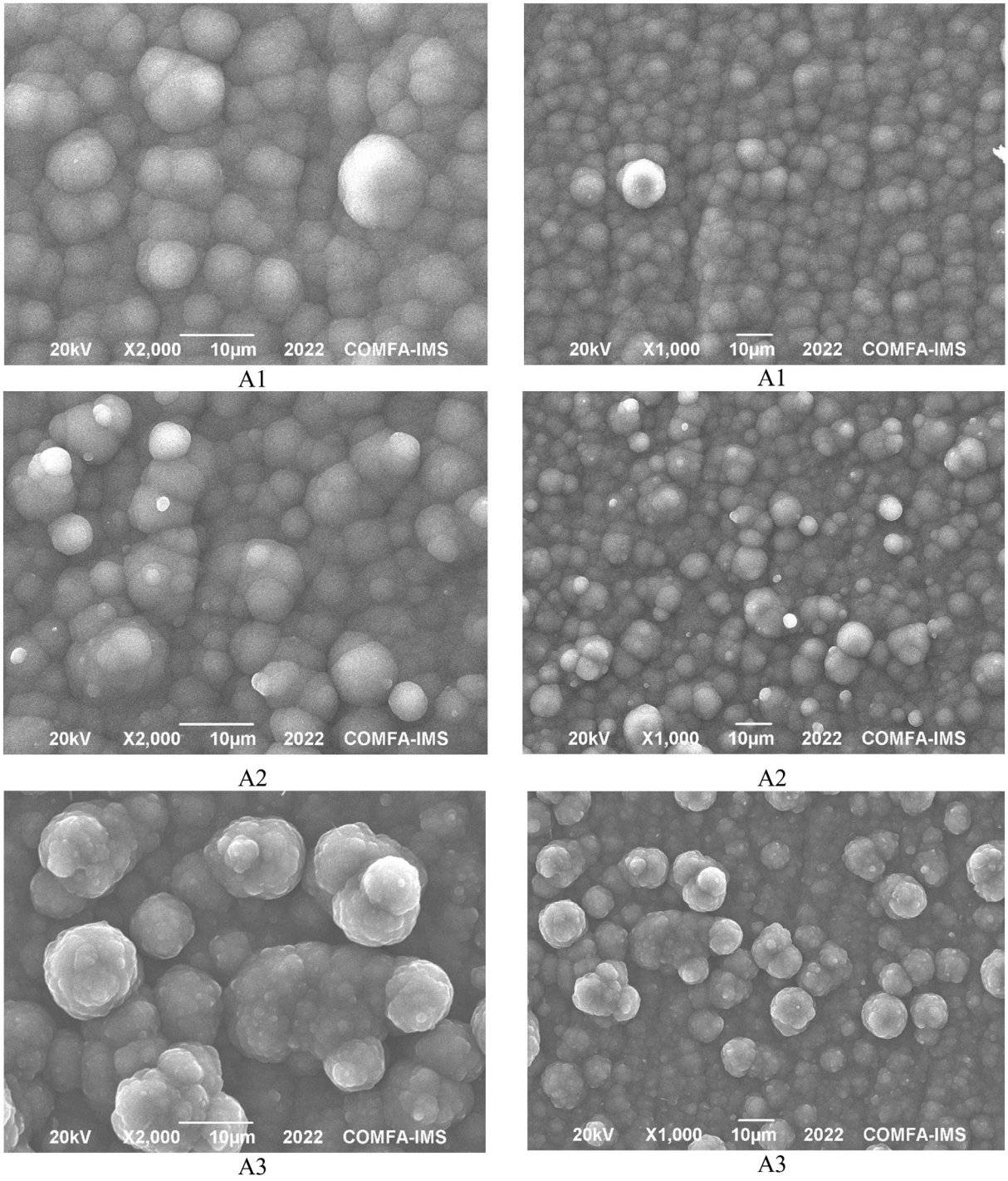


**FIGURE 2** SEM pictures of PPy sample A1, A2 and A3.

**TABLE 2** Raman signals ($cm^{-1}$) of (a) theoretical PPy,[21] (b) practical PPy[22] and doped PPy films.

| PPy (a) in Ref. 21 | PPy (b) in Ref. 22 | A1 | A2 | A3 | Vibration |
|---|---|---|---|---|---|
| 1676 | 1589 | 1580 | 1587 | 1580 | $\upsilon$C═C |
| 1307 | 1328 | 1349 | 1350 | 1321 | $\upsilon$C—N |
| – | – | – | – | 1237 | $\delta$C—C |
| 1049 | 1047 | 1000 | 1005 | 1048 | $\delta$N—H |
| 955 | 976 | 818 | 803 | 832 | $\delta$ ring deformation |

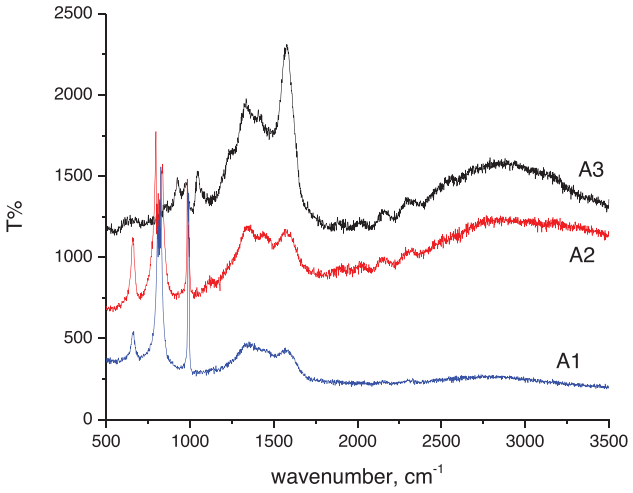


**FIGURE 3** Raman spectra of PPy films.

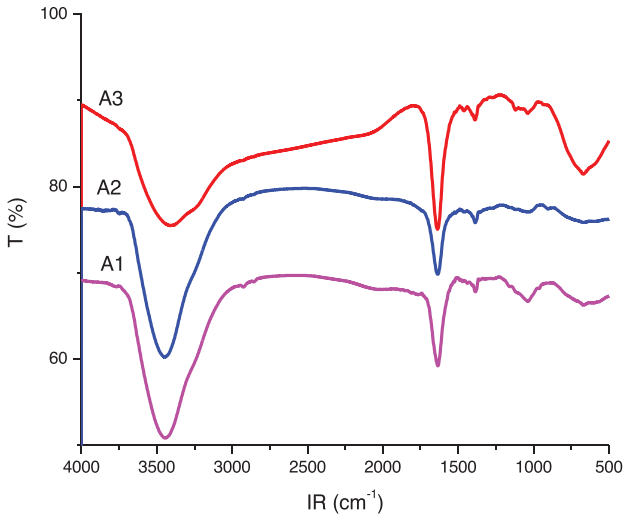


**FIGURE 4** FT-IR spectra of PPy films.

to the Raman data of oxidized PPy determined according to theory and practice (in PPy/$Al_2O_3$ nanocomposite).[21,22] The theoretical results of the Raman shift of PPy films differ from the experimental ones. In addition, the occurrence of the C—C stretching vibration, which is not present in either of the PPy data, was used to demonstrate the presence of 3Nisa in the doped PPy film.

## 3.4 | FTIR spectra

In the FTIR spectra of the A1–A3 samples in Figure 4, N—H, C—H, C═O, C═C, and C═N groups of PPy and 3-nitrosalicylate structures can be observed. The N—H bond in the aromatic vibrations (υN-H) of PPy or the O—H bond in the water molecule were recorded at 3425 $cm^{-1}$ (A1), 3437 $cm^{-1}$ (A2), and 3431 $cm^{-1}$ (A3) stretching vibrations. The C—H stretching vibration was ascribed to the peak at 2931 $cm^{-1}$. At 1635 $cm^{-1}$ (A1), 1631 $cm^{-1}$ (A2), and 1639 $cm^{-1}$ (A3), the vibration of the C═O bond (υC═O) could be noticed.[23–26] At 1543 $cm^{-1}$ (A1), 1550 $cm^{-1}$ (A2), and 1539 $cm^{-1}$ (A3) were υC═C aromatic, and υC═N. The vibration of N—H (δN—H) or O—H (δO—H) was assigned to the band at about 1392 $cm^{-1}$ (A1), 1396 $cm^{-1}$ (A2), and 1430 $cm^{-1}$ (A3). The —$NO_2$ group attributed to the bands at 1045 $cm^{-1}$ (A1), 1053 $cm^{-1}$ (A2), and 1033 $cm^{-1}$ (A3). The aforementioned electrostatic interaction was proved by a minor change in the N—H bending and C═O stretching vibrations. These findings showed that electrochemical doping of 3NiSa with PPy was effective (Figure 4 and Table 3).

**TABLE 3** FTIR signals ($cm^{-1}$) of PPy films.

| Vibration | A1 | A2 | A3 |
|---|---|---|---|
| O—H | 3442 | 3440 | 3419 |
| C—H | 2931 | 2930 | 2929 |
| C═O | 1641 | 1640 | 1639 |
| υC═C aromatic, C═N | 1543 | 1550 | 1539 |
| δN—H, δO—H | 1392 | 1396 | 1430 |
| —$NO_2$ | 1045 | 1053 | 1033 |

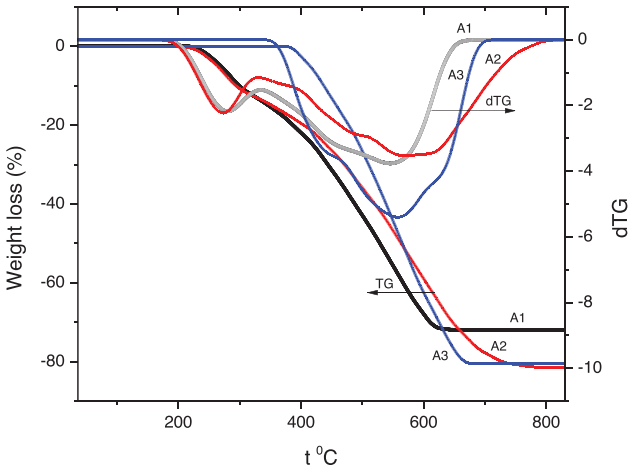


**FIGURE 5** TGA diagrams of the samples A1, A2, and A3.

**TABLE 4** The weight reduces of A1, A2 and A3 samples at different ranges of temperatures.

| Temp (°C) | | ≤200 | 200–400 | 400–600 | ≥600 |
|---|---|---|---|---|---|
| Weight reduction (%) | A1 | 0 | 13.5 | 71.3 | 82.5 |
| | A2 | 0 | 15.27 | 69.06 | 81.2 |
| | A3 | 0 | 10.5 | 71.2 | 80.4 |

## 3.5 | Thermogravimetric analysis of PPy samples

Figure 5 illustrates the results of TGA and DTA analysis on the A1, A2, and A3 samples. The doped PPy films deteriorated in a series of processes that corresponded to

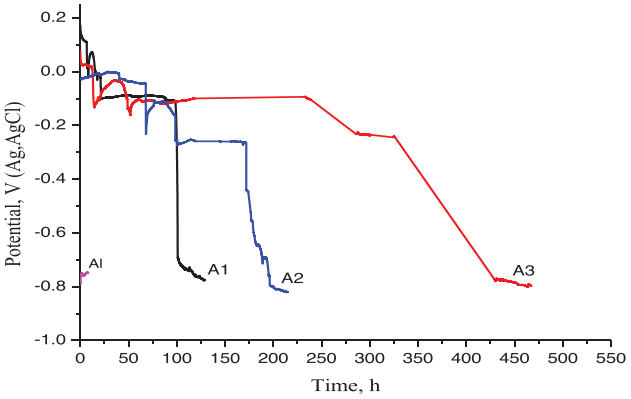


**FIGURE 6** OCP of sample A1, A2, A3, and bare aluminum in 3% NaCl solution.

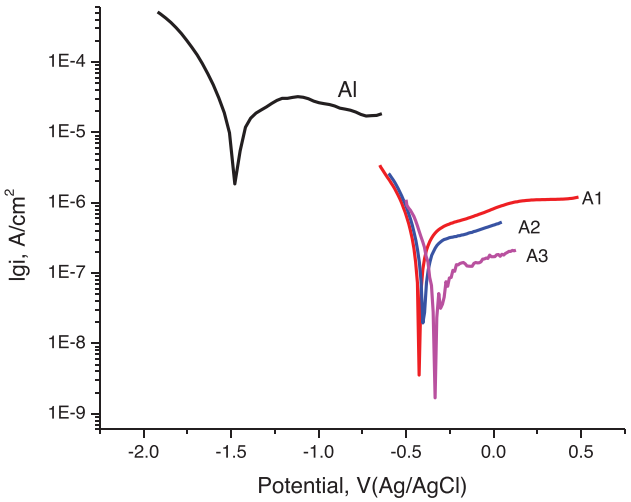


**FIGURE 7** Tafel curves of samples Al, A1, A3, and bare aluminum in 3% NaCl solution.

**TABLE 5** Corrosion parameters of PPy coatings in 3% NaCl solution.

| | Bare Al | A1 | A2 | A3 |
|---|---|---|---|---|
| $I_{corr}$ (μA cm$^{-2}$) | 3.6E-5 | 3.5E-7 | 2.1E-7 | 9.3E-8 |
| $E_{corr}$ (V) versus Ag/AgCl) | −1.47 | −0.41 | −0.39 | −0.32 |

their multiphase structure (PPy, 3-NiSa, oligomers, residual monomer, and other impurities). For example, the decrease in weight induced by water evaporation happened between 20 and 100 °C. The leftover monomer, oligomers, 3-Nisa, and other impurities were, subsequently, degraded at temperatures ranging from 100 to 400 °C. At 400–600 °C, PPy was decomposed via the weight reduction (See Table 4 ).

## 3.6 | Electrochemical study on the doped PPy films on aluminum

In 3% NaCl electrolyte, the PPy samples' open circuit potential (OCP) was measured. The OCP-time curves of A1, A2, A3, and bare aluminum are shown in Figure 6.

With PPy film on Al substrate, the OCP of A1, A2, and A3 were initially positive but declined after a while. PPy coatings might offer steel with barrier protection during immersion. It could be noted that these OCP fluctuated in the positive plateau. This is a particular characteristic of the self-healing behavior. Once the OCP reaches the corrosion

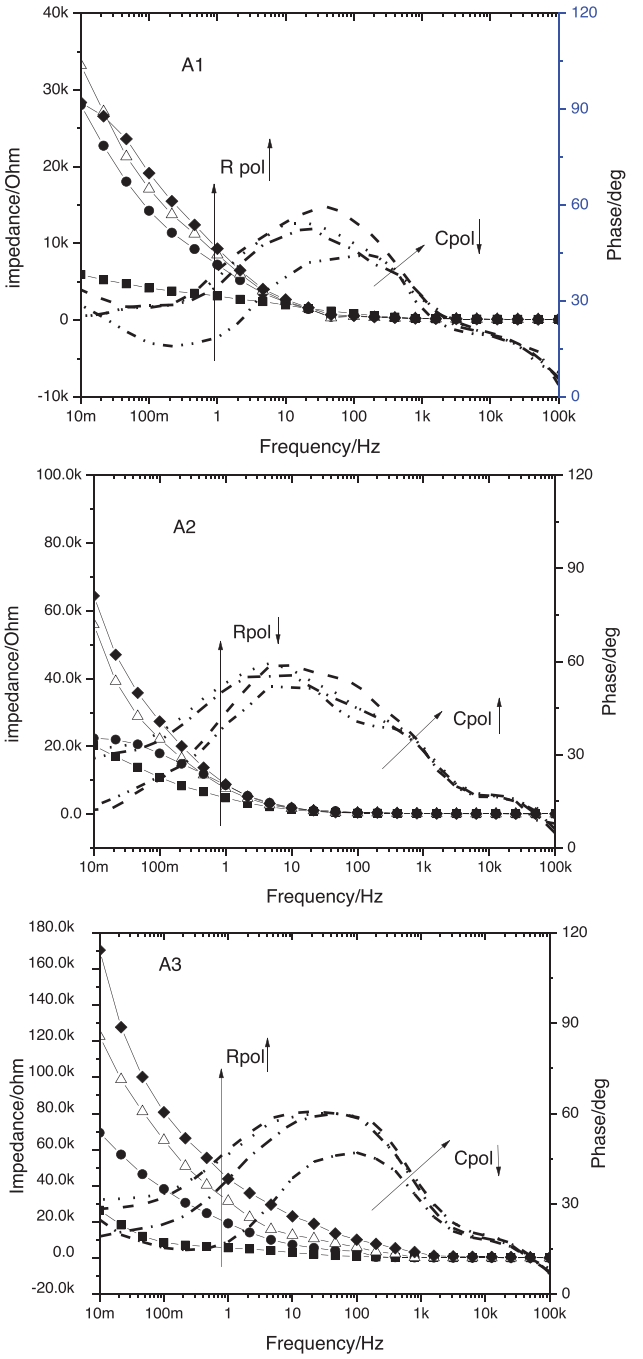


**FIGURE 8** EIS spectra of A1, A2, A3 sample obtained from measurement 3% NaCl solution at −0.3 V (vs SCE) polarization in 0 (■), 30 (●), 60 (Δ), 90 (◆) minutes.

| Time of exposure (h) | A1 sample | A2 sample | A3 sample |
|---|---|---|---|
| 0 |  |  |  |
| 16 |  |  |  |

**FIGURE 9** Pictures of samples A1, A2, A3 after 16 h or exposure in NaCl spray.

potential of aluminum, the PPy coating is no longer able to protect the substrate.

Although the OCP curves of A1, A2, A3 exhibited nearly the same behavior, the protection time of A3 stretched for a longer time than that of A1 and A2 samples. Especially, the positive plateau prolonged more than 300 h. Because of the sufficient concentration of dopants 3Nisa in the PPy film, the coating's resistance was enhanced.

Voltametric polarization experiments in NaCl 3.0% solution were performed to confirm the corrosion parameters revealed by OCP measurements. Figure 7 depicts the Tafel curves of the PPy films. Corrosion parameters, such as corrosion potential ($E_{corr}$), corrosion current density ($I_{corr}$) are summarized in Table 5.

The polarization curve profiles for different coated electrodes after exposure time were identical, signifying that all electrodes exhibit similar electrochemical activity. All the observed $E_{corr}$ values for polymer-coated samples were positively shifted compared to uncoated ones in the polarization experiments, which means all the coatings, to some extent, resist corrosion.

The sample A3 displayed the most positive $E_{corr}$ values and smallest values of $I_{corr}$. The used corrosion potential ($E_{corr}$) measurements can determine a material's corrosion susceptibility in each environment. The higher and more positive the values were, the better stability or protection were. Both properties are indicative of corrosion protection. The corrosion current density ($I_{corr}$) is directly proportional to the corrosion rate at the point of intersection of the anodic and cathodic curves. With A3, $I_{corr}$ decreased to $9.3E^{-8}$ μA $cm^{-2}$ compared to bare Al – $3.6E^{-5}$ μA $cm^{-2}$. Thus, the corrosion protection could reached 99%.

The presence of 3Nisa in the structure of PPy film helps to enhance the protection on the Al substrate due to the complicated protection mechanism. Those mechanisms maybe anodic protection, cathodic protection, controlled inhibitor release and barrier protection.

With EIS measurement, the PPy films were reduced at −0.3 V (vs SCE) in 30 min and EIS curves were obtained. Figure 8 shows the EIS curves of A1, A2, A3 recorded in 3% NaCl solution after 30 min of reduction. All the spectra (Figure 8) are characteristic of a coated metal undergoing pitting corrosion, as they present a characteristic second time constant in the low frequency domain.

It can be seen based on the traditional interpretation, that associates higher values of impedance to a higher resistance to corrosion or higher resistance of polymer film.

The obtained data would indicate clearly that polymer film resistance (Rpol) of A3 sample increased after reduction at −0.3 V (vs SCE). The frequency at which the film changed was around 1 Hz (Figure 8). At the same time, it is clear to see that the capacitance of polymer (Cpol) decreased. It is indicated that 3Nisa anions could release out of PPy film. After 90 min of reduction, the film resistance could be 60 kΩ. PPy film was reduced to become reduced PPy so that conductivity of film was bad. With the samples A1, A2 the changes of film capacitance were not so clear.

The experiments were conducted the same way. There were not the same results with A1, A2 samples. The resistances of PPy films were in small values and the difference between reduction steps were very small. The resistance of films at 1 Hz was 10 kΩ. PPy film capacitance seemed to not change. After 90 min of reductions, the films were totally decomposed and pulled off the substrates.

EIS results showed that A3 sample could be reduced by polarization and produced the dopant anion that inhibited corrosion process.

To confirm the anticorrosive properties of PPy films, salt spray tests were conducted. The pictures of samples were shown in Figure 9.

After a 16-h salt spray exposure test, the samples were analyzed. The samples A1, and A2 showed a significant incursion of around 70%–80% of the overall area, however, the A3 sample did not.

The 16 h of salt spray testing demonstrated the outstanding adherence of sample A3 to the substrate with almost little to no underlayer corrosion. PPy film, thus, is proved to potentially give corrosion resistance to aluminum in the presence of 3Nisa. The key mechanism might be the release of 3NiSA during the protection period (reduction reaction). These results seem to be better than that of PPy films protected carbon steel.[27]

## 4 | CONCLUSIONS

The study successfully electrodeposited polypyrrole (PPy) film on an aluminum substrate with 3-nitrosalicylate (3Nisa) as a dopant. There was no sign of film degradation and the PPy film was durable. The anions 3-nitro salicylate were crucial in the passivation of the mild steel substrate, resulting in a smooth coating and adhesion.

The thermal stability of the doped PPy films was enhanced by using 3-nitrosalicylate anions. Despite its limited mobility, 3-nitrosalicylate might be gradually liberated from the PPy film upon reduction. The 3-nitrosalicylate dopants may improve PPy protection by having self-healing and barrier characteristics. These findings indicate that a PPy film doped with 3-nitrosalicylate anions might serve as an effective corrosion prevention layer.

## ACKNOWLEDGMENTS

This research was funded by the Vietnam National Foundation for Science and Technology Development (NAFOSTED) under grant number 104.02-2019.327.

## ORCID

*Nguyen Thi Bich Viet* https://orcid.org/0000-0001-6383-721X

*Vu Quoc Trung* https://orcid.org/0000-0003-4629-0958

## REFERENCES

1. J. N. Barisci, T. W. Lewis, G. M. Spinks, C. O. Too, G. G. Wallace, Conducting polymers as a basis for responsive materials systems, *J. Intell. Mater. Syst. Struct.* **1998**, *9*, 723.
2. M. Kendig, M. H. L. Warren, "Smart" corrosion inhibiting coatings, *Prog. Org. Coat.* **2003**, *47*, 183.
3. G. Kordas, Conducting polymer coatings for corrosion protection, in *Polymer Coatings: Technologies and Applications*, CRC Press, Boca Raton, FL **2020**, Ch. 10.
4. N. P. Tavandashti, M. Ghorbani, A. Shojaei, J. M. C. Mol, H. Terryn, K. Baert, Y. Gonzales-Garcia, Inhibitor-loaded conducting polymer capsules for active corrosion protection of coating defects, *Corros. Sci.* **2016**, *112*, 138.
5. G. Paliwoda-Porebska, M. Stratmann, M. Rohwerder, K. Potje-Kamloth, Y. Lu, A. Z. Pich, H.-J. Adler, On the development of polypyrrole coatings with self-healing properties for iron corrosion protection, *Corros. Sci.* **2005**, *47*, 3216.
6. A. Michalik, M. Rohwerder, Conducting polymers for corrosion protection: A critical view, *Z. Phys. Chem.* **2005**, *219*, 1547.
7. F. Gao, J. Mu, Z. Bi, S. Wang, Z. Li, Recent advances of polyaniline composites in anticorrosive coatings: A review, *Prog. Org. Coat.* **2021**, *151*, 106071.
8. K. Namsheer, C. S. Rout, Conducting polymers: a comprehensive review on recent advances in synthesis, properties and applications, *RSC Adv.* **2021**, *11*, 5659.
9. V. Q. Trung, H. M. Hung, L. M. D. Le Van Khoe, N. T. B. Viet, D. K. Linh, V. T. Huong, N. D. Dat, D. T. Y. Oanh, N. X. Luong, N. T. Chinh, H. Thai, H. T. T. Lan, C. L. Van, Ş. Ţălu, D. N. Trong, Synthesis and characterization of polypyrrole film doped with both molybdate and salicylate and its application in the corrosion protection for low carbon steel, *ACS Omega* **2022**,*7*, 19842.
10. H. M. Hung, T. M. Thi, L. M. D. Le Van Khoe, H. T. T. Lan, L. T. Hoan, V. T. Xuan, N. T. B. Viet, N. X. Luong, N. T. Chinh, T. Hoang, V. T. Huong, V. Q. Trung, Polypyrrole-based nanocomposites doped with both salicylate/molybdate and graphene oxide for enhanced corrosion resistance on low-carbon steel, *Des. Monomers Polym.* **2023**, *26*, 171.
11. S. H. Cho, H. M Anderson, S. R. White, N. R. Sottos, P. V. Braun, Polydimethylsiloxane-based self-healing materials, *Adv. Mater.* **2006**, *18*, 997.
12. F. Zhang, P. Ju, M. Pan, D. Zhang, Y. Huang, G. Li, X. Li, Self-healing mechanisms in smart protective coatings: A review, *Corros. Sci.* **2018**, *144*, 74.
13. Y. Yin, M. Schulz, M. Rohwerder, Optimizing smart self-healing coatings: Investigating the transport of active agents from the coating towards the defect, *Corros. Sci.* **2021**, *190*, 109661.
14. D. G. Shchukin, M. Zheludkevich, K. Yasakau, S. Lamaka, M. G. S. Ferreira, H. Mohwald, Layer-by-layer assembled nanocontainers for self-healing corrosion protection, *Adv. Mater.* **2006**, *18*, 1672.
15. G. Paliwoda-Porebska, M. Rohwerder, M. Stratmann, U. Rammelt, M. D. Le, W. Plieth, Release mechanism of electrodeposited polypyrrole doped with corrosion inhibitor anions, *J. Solid State Electrochem.* **2006**, *10*, 730.
16. A. Vimalanandan, L. P. Lv, T. H. Tran, K. Landfester, D. Crespy, M. Rohwerder, Redox-responsive self-healing for corrosion protection, *Adv. Mater.* **2013**, *25*, 6980.
17. Y. Yin, M. Prabhakar, P. Ebhinghaus, C. C. Silva, M. Rohwerder, Neutral inhibitor molecules entrapped into polypyrrole network for corrosion *protection*, *Chem. Eng. J.* **2022**, *40*, 135739.
18. S. Kanwal, Z. Akhter, N. Z. Ali, R. Hussainb, S. Qamara, Corrosion protection of aluminum alloy (AA2219- 6) using sulfonic acid-doped conducting polymer coatings, *New J. Chem.* **2022**, *46*, 14557.
19. K. M. Cheung, D. Bloor, G. C. Stevens, Characterization of polypyrrole electropolymerized on different electrodes, *Polymer* **1998**, *29*, 1709.

20. V. Q. Trung, T. H. Hanh, T. H. Quang, H. M. Hung, D. K. Linh, H. T. T. Lan, L. M. Duc, Corrosion protection of molybdate doped polypyrrole film prepared in succinic acid solution, *Corros. Eng. Sci. Technol.* **2018**, *53*, 59.
21. D. E. Tallman, K. L. Levine, C. Siripirom, V. G. Gelling, G. P. Bierwagen, S. G. Croll, Nanocomposite of polypyrrole and alumina nanoparticles as a coating filler for the corrosion protection of aluminum alloy 2024-T3, *Appl. Surf. Sci.* **2008**, *254*, 5452.
22. M. J. L. Santos, A. G. Brolo, E. M. Girotto, Study of polaron and bipolaron states in polypyrrole by in situ Raman spectroelectrochemistry, *Electrochim. Acta* **2007**, *52*, 6141.
23. A. Faulques, W. Wallnoefer, H. Kuzmany, Vibrational analysis of heterocyclic polymers: a comparative study of polythiophene, polypyrrole, and polyisothianaphtene, *J. Chem. Phys.* **1989**, *90*, 7585.
24. P. Moarref, M. Pishvaei, A. Soleimani-Gorgani, F. Najafi, Synthesis of polypyrrole/indium tin oxide nanocomposites via miniemulsion polymerization. *Des. Monomers Polym.* **2016**, *19*, 138.
25. Y. Chena, L. Song, Z. Chen, L. Zhang, W. Wu, Morphology and properties of polypyrrole/cyclodextrin nanowires sing molecular templates. *Des. Monomers Polym.* **2015**, *18*, 35.
26. Q. Zhu, E. Li, X. Liu, W. Song, Y. Li, X. Wang, C. Liu, Epoxy coating with in-situ synthesis of polypyrrole functionalized graphene oxide for enhanced anticorrosive performance, *Prog. Org. Coat.* **2020**, *140*, 105488.
27. H. M. Hung, D. K. Linh, N. T. Chinh, L. M. Duc, V. Q. Trung, Improvement of the corrosion protection of polypyrrole coating for CT3 mild steel with 10-camphorsulfonic acid and molybdate as inhibitor dopants, *Prog. Org. Coat.* **2019**, *131*, 407.

**How to cite this article:** L. V. Khoe, H. M. Hung, L. M. Duc, N. X. Luong, N. T. B. Viet, V. T. Huong, D. T. Y. Oanh, V. Q. Trung, Properties and corrosion protection of polypyrrole prepared by electrochemical polymerization on aluminum, *Vietnam J. Chem.* **2024**, *62*, 412. https://doi.org/10.1002/vjch.202400003